eXPRESS Polymer Letters Vol.14, No.2 (2020) 115–133
Available online at www.expresspolymlett.com
https://doi.org/10.3144/expresspolymlett.2020.11

Novel processing of polyhydroxybutyrate with micro- to nanofibrillated cellulose and effect of fiber morphology on crystallization behaviour of composites

V. K. Rastogi[1*], *P. Samyn*[2]

[1]Department of Bioproducts and Biosystems, School of Chemical Technology, Aalto University, Vuorimiehentie 1, 02150 Espoo, Finland
[2]Hasselt University, Institute for Materials Research, Applied and Analytical Chemistry, Agoralaan Gebouw D, B-3590 Diepenbeek, Belgium

Received 2 June 2019; accepted in revised form 23 July 2019

Abstract. In this work, the intrinsic drawbacks of polyhydroxybutyrate (PHB) such as slow crystallization rate, secondary crystallization and brittle nature were improved by blending with bio-based fillers, i.e. nanofibrillated/microfibrillated cellulose (NFC/MFC). A novel chlorinated-solvent-free based system was developed to blend PHB and NFC/MFC that resulted in homogenous dispersion of fibers in the PHB matrix, without the need for surface modification of fibers. The developed nano/micro-composite materials were fabricated as masterbatch pellets and films. Additionally, the effect of different NFC/MFC fiber morphologies influencing the crystallization behaviour of PHB was investigated in detail by differential scanning calorimetry, polarized optical microscopy and Fourier transform infrared spectroscopy. Both non-isothermal and isothermal crystallization studies (modelled with Avrami's kinetics) were performed on nanocomposites and variations in crystallization kinetics of PHB after addition of NFC/MFC were determined. Addition of NFC/MFC resulted in the drastic increase in the crystallization rate of PHB and hence they acted as nucleating agents. The fine and homogeneous morphology of NFC produced smaller PHB spherulites and restricted the growth of secondary crystals, hence resulted in more flexible films than PHB or PHB-MFC films, as determined by the mechanical testing of films. The more heterogeneous morphology of MFC altered the PHB crystallization mechanism most, as seen from the distorted shape of PHB spherulites along with the higher Avrami exponent, *i.e.* $n \geq 3$.

Keywords: *nanocomposites, processing technologies, micro/nanofibrillated cellulose, polyhydroxybutyrate, crystallization kinetics*

1. Introduction

Polyhydroxybutyrate (PHB) is the simplest form of polyhydroxyalkanoates, produced via fermentation of carbon substrates such as sugars, renewable waste feedstock including agricultural waste, organic waste, municipal solid waste, and paper mill sludge [1]. PHB is a water insoluble, biodegradable, biocompatible, and thermoplastic material, competing strongly with other commercially known bioplastics. However, its brittleness, high stiffness, high crystallinity, and narrow processing window restrict the applications of PHB as a packaging or coating material. Secondary crystallization in PHB is considered the principal reason for PHB brittleness [2]. In addition, low nucleation density and slow crystallization rate are also associated with the formation of large spherulites inducing cracks, which deteriorate mechanical properties of PHB [2, 3]. Therefore, several methods were reported to improve the properties of PHB such as (i) using copolymers [4, 5], or (ii) physical blending

*Corresponding author, e-mail: vibhore.rastogi@aalto.fi

with additives. Numerous approaches were used for blending such as addition of plasticizers [6, 7], nucleating agents [8–10], fillers [11, 12], along with few nano-scale additives such as nano-clays [13, 14] and carbon nanotubes [15]. In respect of the bio-based nature of PHB, there is need for better controlling its properties by using bio-based fillers, which opens up new possibilities for the formulation of fully bio-based and biodegradable PHB composite.

Blending of PHB with native cellulose fiber [16], flax [17], wheat straw fiber [18] was practiced to influence the crystallization mechanisms and hence mechanical properties of PHB, but blending with cellulose micro/nano-crystals (MCC/CNC) is very recent [11, 19, 20]. In addition, nanofibrillated/microfibrillated cellulose (NFC/MFC) fibers also possess excellent reinforcing ability along with excellent oxygen barrier properties [21, 22] but were rarely used as an additive for improving PHB properties. In order to utilize the advantages offered by NFC/MFC (polar nature), however, a uniform fiber distribution within non-polar PHB matrix is necessary. As such, surface modification of MFC/NFC was the most favourable route for achieving most distributive mixing [23–25]. In addition, solvent processing of PHB in the conventional toxic organic solvents such as chloroform, dichloromethane, and dimethylformamide was often required to maximize the fiber distribution in polymer matrix [13, 26]. Alternatively, propylene carbonate (PC) as a dipolar aprotic solvent with valuable properties such as non-corrosive, less toxic and biodegradable nature offers a more 'green' and environmental friendly image that has been considered as an alternative to the highly aggressive chlorinated solvents [27, 28]. Propylene carbonate has been effectively used to extract the PHB from the microorganisms and considered better than chloroform [27]. Due to its high boiling point and non-volatile nature, it can be recycled and reused several times [29]. Additionally, due to the high dielectric constant less amount of propylene carbonate is used to process PHB comparing to chloroform [29]. Still to date, the interesting polar-aprotic nature of propylene carbonate has not been further explored to mix the polar fibers (NFC/MFC) with non-polar PHB.

In addition to the blending procedures used for the uniform fiber distribution in PHB, fiber morphology also influences the crystallization behaviour of polymer composites. Siqueira *et al*. [30] has shown the influence of modified CNC/MFC addition (12 wt%) on the crystallization kinetics of polycaprolactone (PCL). In presence of CNC and to a lesser extent MFC, the crystallinity index of the matrix increases, suggesting a nucleating effect of the cellulose fillers in relation to surface area. It was determined that the coarse and highly entangled structure of MFC limits the mobility of PCL chains and results in reduced crystallinity, compared to CNC with fine morphology that can be easily displaced to accommodate polymer crystallization. In contrast, MFC resulted in faster crystallization of PCL than CNW, by requiring lowest bulk activation energy to crystallize PCL compared to CNW. Other studies also mentioned the favourable nucleating abilities of MFC or CNC for various polymer matrixes like poly(oxyethylene) (PEO) [31] and polylactic acid (PLA) [32]. All of the above stated polymer-fiber composites showed improvement in the crystallization behaviour only when the fiber fraction equals or is greater than 10 wt%. In contrast to that, there are limited studies emphasizing the need to lower the nano/micro-filler amount in order to achieve the best possible properties for the polymer matrix [33, 34]. Especially, when unmodified CNC was first dispersed in polyethylene glycol (PEG) and then introduced in PHB matrix, a homogenous distribution of CNC was achieved up to 0.45 wt% that dramatically reduced the brittleness of nanocomposite films, while, further addition of 0.75 wt% resulted in the adverse properties due to over-loading of additive [34]. Consequently, it seems that a lower fraction of nano/micro fibers might be sufficient to induce the required physical and crystalline properties of a polymer matrix, provided the uniform distribution of additive material.

In this work, a novel chlorinated-solvent-free based approach was developed to blend PHB with small fiber fractions of nanofibrillated cellulose (NFC) and microfibrillated cellulose (MFC), in order to influence the PHB intrinsic crystallization processes and hence its mechanical properties. A detailed study on crystallization behaviour/kinetics of the PHB nanocomposites was made by using thermal analysis and fitting of the Avrami model. The PHB-NFC/MFC nanocomposites were characterized as masterbatch pellets and further processed into free-standing films by compression moulding. The influences of NFC/MFC morphology on the crystallization rate, crystallinity and the mechanical properties were determined in subsequent steps.

2. Experimental method

2.1. Materials

The PHB pellets were purchased from Metabolix GmbH (Köln, Germany) having the trade name of Mirel M2100 with a molecular weight M_w = $3.7 \cdot 10^5$ g/mol and polydispersity (M_w/M_n) in between 1.60 and 1.85. A never-dried microfibrillated cellulose (MFC, Arbocel P1011, 20% consistency) was obtained from Rettenmaier GmbH (Rosenberg, Germany) and a never-dried nanofibrillated cellulose suspension (NFC, E167, 2% consistency) was supplied by VTT Technical Research Centre of Finland (Espoo, Finland). Polyethylene glycol (PEG, average molecular weight of 200 g/mol, purity 98.0%) and propylene carbonate (PC, average molecular weight of 102 g/mol, purity 99.0%) were purchased from Sigma Aldrich Chemical Ltd. Teflon foils of thickness 100–400 μm were kindly provided by Dyneon GmbH (Germany).

2.2. Processing of PHB-NFC/MFC masterbatches

Propylene carbonate (PC) was used as a solvent to dissolve PHB while polyethylene glycol (PEG) was used as a dispersing agent for NFC and MFC. A low molecular weight PEG 200 was selected in order to ensure the complete mixing in PHB matrix that would further facilitate the homogeneous dispersion of NFC/MFC in PHB matrix, as PHB/PEG miscibility decreased with the increasing molecular weight of PEG like for 1500 and 3400 g/mol [35]. PHB pellets were first solubilized in propylene carbonate (25%, w/v) at a temperature of 140 °C under constant overhead stirring, until the polymer dissolved completely. In parallel, suspensions of NFC/MFC with variable fiber fractions were prepared in a mixture of PEG/water (1.60:1) and ultrasonicated for 2 minutes at 50% power, in order to obtain homogenous suspensions. All formulations were adjusted with the same amount of PEG and water. The prepared suspensions of NFC and MFC were mixed accordingly with PHB-PC solution slowly at 140 °C for 5 minutes under continuous stirring in order to obtain a fiber fraction of 0, 0.25, 0.50, 1, 2 and 5 wt% in PHB matrix (on dry fiber basis). The prepared suspensions of PHB and NFC/MFC were poured in an in-house made noodle former device and left for solidification at ambient conditions for 30 mins. The suspensions were later squeezed into a cold water at 4 °C and the resulting thin noddle shape composite material is referred as masterbatch (MB). Due to the non-volatile nature of PC and PEG (unlike chlorinated solvents), masterbatches were subjected to five consecutive hot water washing cycles to diffuse out the solvents completely. Later, all masterbatches were dried at 80 °C for 24 hours in an air-circulatory oven for complete water removal. All prepared PHB-NFC/MFC compositions are presented in Table 1 and same conventions will be used for masterbatches and films (see 2.3). As a reference material, PHB was processed

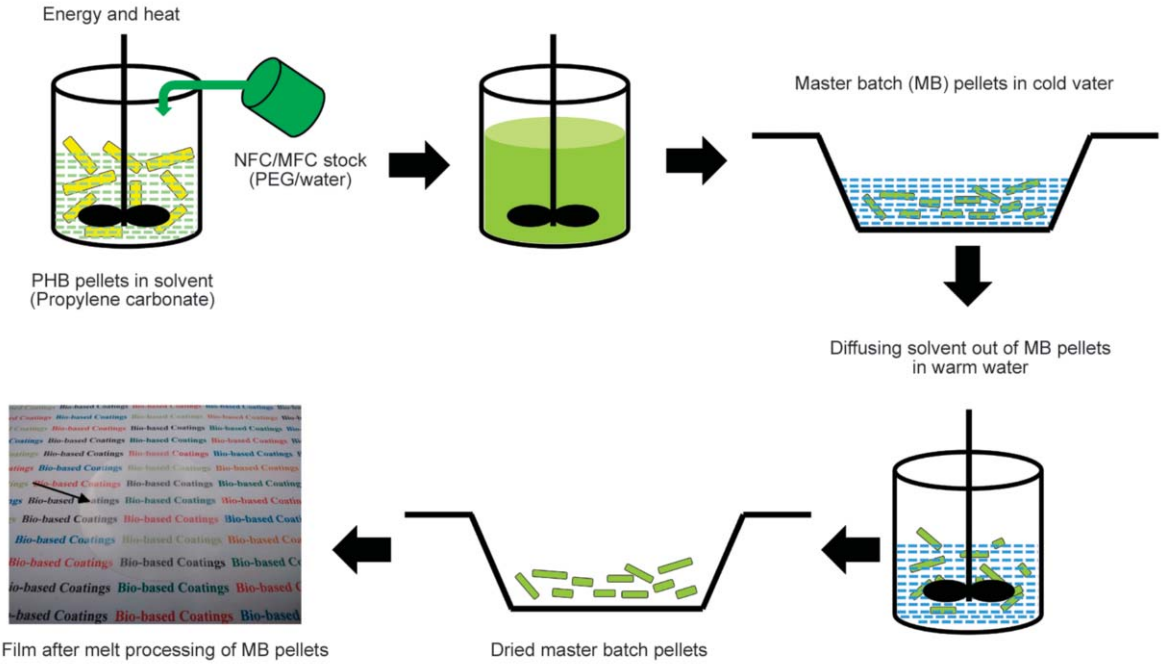

Figure 1. Schematic for preparing PHB-NFC/MFC masterbatch and films.

Table 1. Formulations of PHB-NFC/MFC masterbatches and films.

Fiber fraction in PHB matrix [wt%]	PHB	NFC	MFC
0	P-PHB	–	–
0.25	–	NFC 0.25	MFC 0.25
0.50	–	NFC 0.50	MFC 0.50
1.00	–	NFC 1.00	MFC 1.00
2.00	–	NFC 2.00	MFC 2.00
5.00	–	–	MFC 5.00

similarly in presence of PEG/water with no NFC/MFC and is termed as processed-PHB or P-PHB. A schematic diagram of the complete processing route of PHB with NFC/MFC is presented in Figure 1.

2.3. Fabrication of PHB-NFC/MFC films

The dried masterbatches were compression moulded in a hydraulically heated press (LaboPress P 200 S, Vogt Maschinenbau GmbH) between the two Teflon sheets at 180 °C. Masterbatches were first pressed for 1.5 minutes without any pressure and subsequently pressed for additional 10 seconds with a pressure of 50 bars. After hot pressing, the films were cooled at ambient conditions and removed from the Teflon sheets. For each film, 500 mg of masterbatch material was used, resulting in comparable thickness of the films of 50 to 80 μm.

2.4. Characterization of PHB-NFC/MFC masterbatches and films

The variations in the surface morphology of pure MFC and NFC were determined through scanning electron microscopy (SEM), using Hitachi tabletop microscope (TM 3000, Hitachi, Krefeld, Germany) at various magnifications. Further, the topography of MFC and NFC at nanoscale was studied with tapping-mode atomic force microscopy (AFM), using Nanoscope III with a tube scanner from Digital Instruments (Veeco, Santa Barbara, CA, USA) and silicon tips with stiffness k = 50 N/m and resonant frequency of 360 kHz (PPP-NCH, Nanoandmore, Wetzlar, Germany).

The thermal properties of PHB-NFC/MFC masterbatches were determined by differential scanning calorimetry (DSC 8500, PerkinElmer, Rodgau, Germany) and used further to derive the crystallization behaviour/kinetics of composites. All experiments were performed under a constant nitrogen gas flow. The non-isothermal crystallization process was carried out according to the following procedure. Each sample weight of 5 mg (sealed in aluminium pans) was subjected to two heating cycles with an intermediate cooling cycle. During the first heating cycle, samples were heated from –40 to 200 °C at a heating rate of 10 °C/min to erase the thermal history of the samples. After being kept at 200 °C for 2 mins, the molten sample was cooled to –40 °C at a cooling rate of 30 °C/min and kept for 2 mins. Subsequently, the sample was heated again from –40 to 200 °C at a heating rate of 10 °C/min. The first cooling and second heating cycles of the thermograms were used to analyse the thermal properties. The glass transition temperature (T_g), melting temperature (T_m) and melting enthalpies (ΔH_m) were determined from the second melting peak with the maximum peak temperature (T_{m2}). The melt crystallization temperatures (T_{mc}) were determined from the cooling cycle. The degree of crystallinity (X_c) of samples was evaluated by the Equation (1) to examine the changes in the overall crystallinity of PHB with the addition of different fibers [13]:

$$X_c = \frac{\Delta H_m}{\Delta H_m^\circ \left(1 - \frac{\text{wt\% } filler}{100}\right)} \cdot 100 \quad (1)$$

where ΔH_m represents the melting enthalpy of the crystals formed in the polymer, ΔH_m° is the theoretical enthalpy value for a 100% crystalline PHB equalling 146 J/g [13], wt% filler is the mass fraction of fibers present in the PHB masterbatch, and X_c is the crystallinity of the polymer present in the composite. The measurements were repeated 3 times per sample and reported as average values with the statistical standard deviation.

For the isothermal crystallization process, following procedure was used. Each sample weight of 5 mg (sealed in aluminium pans) was heated to 200 °C at the heating rate of 10 °C/min and kept there for 2 mins to erase the previous thermal history. They were then quenched to the crystallization temperature of 80 °C at the cooling rate of 100 °C/min. The isothermal step was maintained at that temperature during the entire crystallization process for at least 6 min. The heat flow during the crystallization was recorded as the function of time and Avrami parameters (n and k) were calculated using the Origin® software by following the method of Lorenzo *et al*. [36]. The half crystallization time ($t_{1/2\ Iso}$) was measured directly from the experimental raw data of isothermal crystallization measurements and compared with the calculated half crystallization time ($t_{1/2\ Avrami}$) obtained

from the Avrami parameters. The measurements were repeated 3 times per sample and reported as average values with the statistical standard deviation.

The fracture morphology of PHB-NFC/MFC films was characterized on cross sections of the film by scanning electron microscopy (SEM), using Hitachi tabletop microscope (TM 3000, Hitachi, Krefeld, Germany) at various magnifications. The films were fractured after cooling in liquid nitrogen. For better resolution, the films were coated with a thin gold layer.

Spherulite morphology of PHB-NFC/MFC films was visualized by polarized light optical microscopy (POM) taken with a microscope equipped with a digital camera (Axioplan 2, Zeiss, Jena, Germany). Prior to observations, all films were kept for 7 days in vacuum oven to achieve the maximum crystallization [37].

The chemical composition of PHB-NFC/MFC films was determined by attenuated total reflection Fourier-transform infrared spectroscopy or ATR-FTIR on a diamond/ZnSe crystal (9 bounces) (Spectrum 65, Perkin-Elmer, Rodgau, Germany), collecting spectra between 4000 and 550 cm^{-1} wavelengths with a resolution of 4 cm^{-1} and averaged over 32 scans.

Tensile strength tests were performed on PHB-NFC/MFC films using a Universal tensile testing machine (SmarTens 005, KARG Industrietechnik, Germany) with a crosshead speed of 1 $mm \cdot sec^{-1}$. Rectangular shaped samples of films were cut with a die (film thickness = 50–80 μm, gage length = 25 mm and width = 10 mm) and kept for 7 days in vacuum oven and later tensile strength (σ_{max}), Young's modulus (E), and the percentage elongation (ε_b) of films were determined. The measurements were repeated 10 times per sample and reported as average values with the statistical standard deviation.

3. Results and discussions

3.1. Morphological analysis of MFC and NFC

The microscale morphology of freeze-dried MFC and NFC pulp was analyzed by SEM as shown in Figure 2. As seen qualitatively, the morphology of

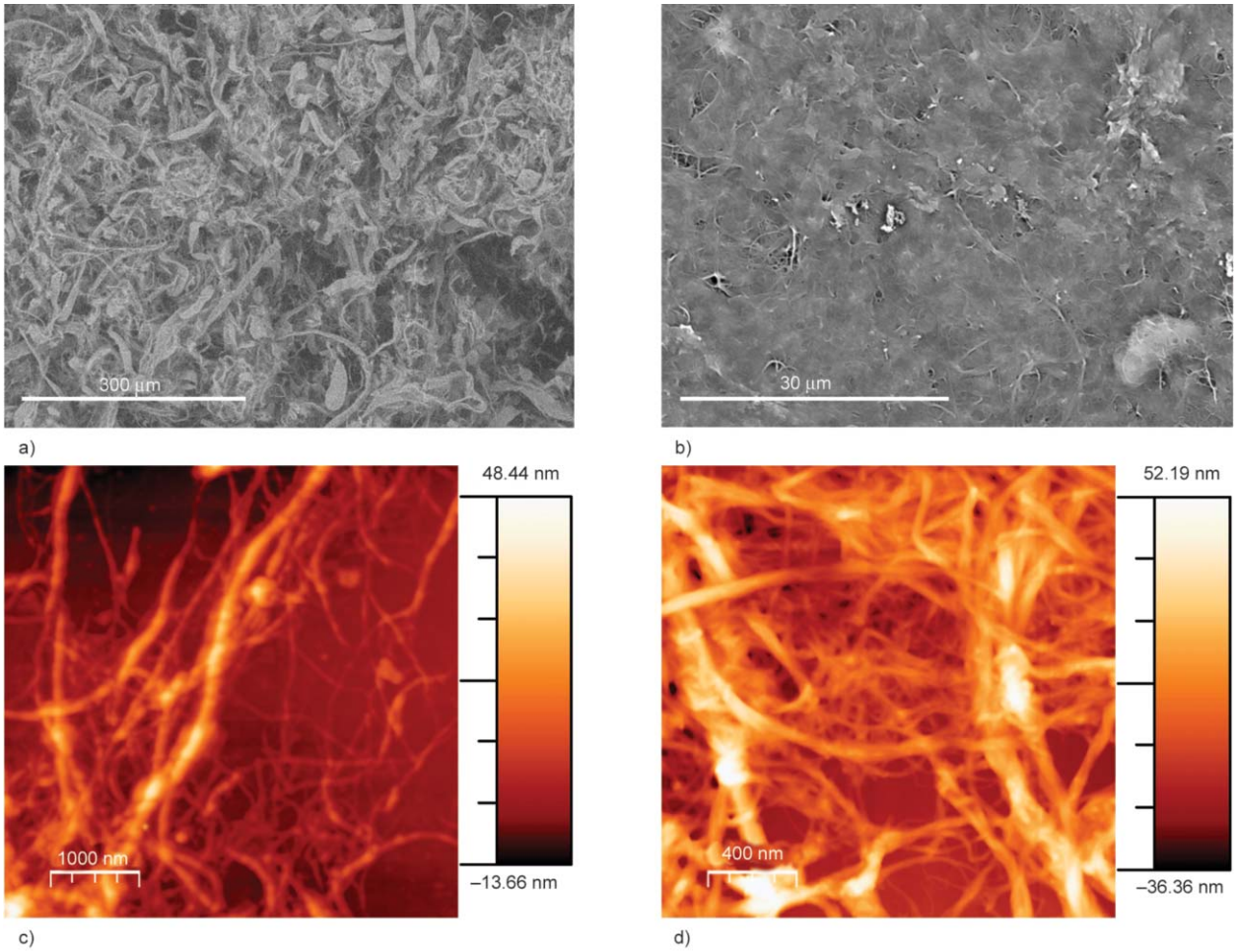

Figure 2. Scanning electron micrographs of freeze-dried pulp flakes of (a) MFC and (b) NFC. AFM height images of (c) MFC and (d) NFC (note the different scales of magnification for the best representation of the MFC and NFC morphology).

MFC (Figure 2a) and NFC (Figure 2b) showed considerable differences attributed to the fiber processing by manufacturers. The MFC fibers had relatively large diameters in parallel with large size variations, while the NFC fibers had relatively thin fiber diameters with more homogeneous sizes forming a fine and dense fiber network. In addition, the nanoscale fiber fraction of MFC (Figure 2c) and NFC (Figure 2d) was visualized by AFM. It was confirmed that MFC rather possessed a combination of fine fiber fractions along with micro-sized fibers. The fiber diameters were altogether quantified by software analysis (Image-J 1.47v), measuring the diameter of 150 random fibers on 6 different SEM and AFM micrographs. For MFC, around 90% diameter lies in a broad range of 0.5–20 μm and only 10% diameter lies in 0.15–0.5 μm interval, whereas, fiber diameters of NFC lies in a narrow range of 40–120 nm with 90% of the fiber diameter below 100 nm. Usually, due to the severe mechanical treatment of native fibers followed by post-separation, the variation in NFC fiber morphology is small which defines the NFC as a homogenous material [38]. Whereas, in case of MFC, less severe mechanical treatment results into bigger aggregates of elementary fibrils and even after the post-separation of treated fibers the morphological difference between the MFC fibers remains large with less homogeneity than NFC [38]. Therefore, NFC could act as a better additive than MFC for influencing the various properties of a polymer matrix like crystallinity that would lead to a composite with isotropic properties.

3.2. Non-isothermal crystallization of PHB-NFC/MFC masterbatches

The crystallization behaviour of neat PHB and the masterbatches with variable fiber fractions of NFC/MFC was investigated by DSC non-isothermal crystallization with first cooling and second melting curves as shown in Figure 3. Table 2 summarizes the thermal parameters from the DSC curves, such as glass transition temperature (T_g), onset crystallization temperature (T_{onset}), melt crystallization temperature (T_{mc}), cold crystallization temperature (T_{cc}), melting enthalpies (ΔH_m), and derived parameters such as half crystallization time ($t_{1/2}$), crystallization rate (R) and crystallinity (X_c). The half crystallization time and crystallization rate were obtained by using the Equation (2) [13] and Equation (3), respectively:

$$t_{1/2\ \mathrm{Non-Iso}} = \frac{T_{onset} - T_{mc}}{\varphi} \tag{2}$$

$$R = \frac{1}{t_{1/2}} \tag{3}$$

where T_{onset} is the temperature at which the crystallization is just started during the cooling cycle, T_{mc} is the peak temperature of the crystallization endotherm, φ is the cooling rate at 30 °C/min, $t_{1/2\ \mathrm{Non\text{-}Iso}}$ represents the time when 50% of the polymer already being crystallized and R represents the crystallization rate.

From Figure 3, few differences were observed in the crystallization behaviour of neat PHB and processed PHB (P-PHB). From the cooling cycle (Figure 3a), the melt crystallization peak was absent for the neat PHB while it was slightly developed in P-PHB. From the heating cycle (Figure 3b), the cold crystallization peak of P-PHB shifted toward the lower temperature in comparison to the neat PHB (see Table 2). These differences are indicating the favourable effects of solvents for PHB processing that might initiated the early crystallization of PHB by reorganizing the polymeric chains [39]. Specifically, a low molecular weight PEG 400 is known as an effective solvent for PHB, lowering the surface energy of chain folding and hence favours the PHB crystallization [40]. However, almost similar degree of crystallinity (X_c) was obtained for both PHB and P-PHB, indicating unaltered crystallization mechanism of PHB when processed by solvents.

The effect of NFC/MFC in the PHB matrix was clearly visualized as a well-developed additional melt crystallization peak comparing to the neat PHB (Figure 3a and 3c). Increasing the fiber fraction (both NFC and MFC) resulted a continuous increase in melt crystallization temperature (T_{mc}) up to the threshold fiber concentration (2 wt% for MFC) that later decreased with the further addition of fibers, i.e. for 5 wt% MFC (Table 2). It should be noted that a maximum of 2 wt% NFC and 5 wt% MFC could be successfully added in PHB matrix as further addition would resulted in the restriction of mixing due to increased viscosity of solution. Clearly, the crystallization of the masterbatches becomes easier in presence of both NFC and MFC, acting as effective nucleating agents and hence improving the crystallization behaviour of PHB. Similarly, an increase in the crystallization rate (R) was evidenced for all PHB-NFC/MFC masterbatches, but again it decreased with the

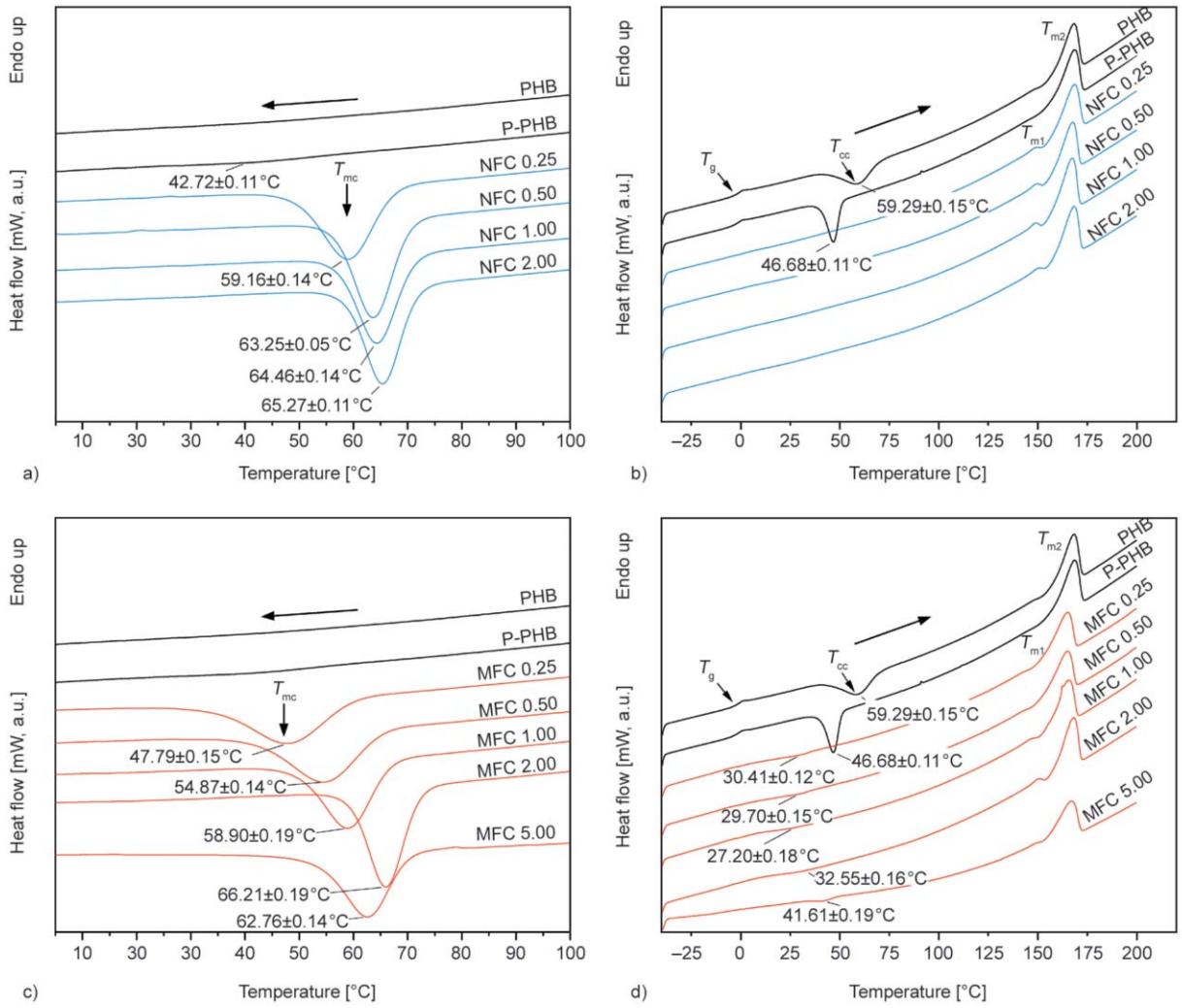

Figure 3. Non-isothermal DSC curves for neat PHB, P-PHB and PHB-NFC/MFC masterbatches showing (a) cooling cycle for PHB-NFC masterbatches, (b) second heating cycle for PHB-NFC masterbatches, (c) cooling cycle for PHB-MFC masterbatches, and (d) second heating cycle for PHB-MFC masterbatches.

Table 2. Non-isothermal crystallization parameters of PHB, P-PHB and PHB-NFC/MFC masterbatches with different fiber concentration of 0.25, 0.50, 1, 2 and 5 wt%.

Sample	T_g [°C]	T_{onset} [°C]	T_{mc} [°C]	$t_{1/2\ Non\text{-}Iso}$ [min]	T_{cc} [°C]	ΔH_m [J/g]	X_c [%]	R [min^{-1}]
PHB	–1.02±0.01	–	–	–	59.29±0.15	51.14±0.02	35.03±0.02	–
P-PHB	–1.05±0.02	53.15±0.15	42.72±0.11	0.348±0.001	46.68±0.11	51.19±0.01	35.06±0.01	2.87±0.01
NFC 0.25	–	67.60±0.11	59.16±0.14	0.281±0.001	–	53.79±0.03	36.94±0.02	3.56±0.01
NFC 0.50	–	70.33±0.02	63.25±0.05	0.236±0.001	–	54.46±0.04	37.68±0.03	4.24±0.01
NFC 1.00	–	71.38±0.17	64.46±0.14	0.231±0.001	–	51.92±0.03	35.74±0.02	4.34±0.02
NFC 2.00	–	71.51±0.21	65.27±0.11	0.208±0.003	–	50.40±0.04	35.23±0.03	4.80±0.07
MFC 0.25	–	59.42±0.21	47.79±0.15	0.388±0.002	30.41±0.12	49.41±0.02	34.01±0.01	2.58±0.01
MFC 0.50	–	65.58±0.23	54.87±0.14	0.357±0.003	29.70±0.15	50.54±0.03	34.70±0.02	2.80±0.02
MFC 1.00	–	66.78±0.15	58.90±0.19	0.263±0.001	27.20±0.18	50.56±0.05	34.98±0.03	3.81±0.02
MFC 2.00	–	72.34±0.16	66.21±0.19	0.204±0.001	32.55±0.16	50.49±0.03	35.29±0.02	4.90±0.02
MFC 5.00	–	70.46±0.25	62.76±0.14	0.257±0.004	41.61±0.19	38.12±0.06	27.48±0.05	3.90±0.05

higher fiber content (5 wt% MFC) and attributed to the restriction in the movement of polymer chain due to fiber overloading. Conversely, half crystallization times ($t_{1/2\ Non\text{-}Iso}$) first decreased up to a minimum value and then increased upon the NFC/MFC addition in the PHB masterbatches (see Table 2). It is

interesting to note that even a low concentration of NFC (0.25 wt%) can act as an efficient nucleating agent in increasing the crystallization of PHB, comparing with MFC at the same concentration. This effect is attributed to the homogeneous blending of PHB and NFC with finer morphology, which acted as free nuclei of smaller size to achieve the uniform and homogeneous PHB crystallization, whereas the MFC fibers were more heterogeneous [22]. Similar observations were noted when PHB was blended with MCC/CNC at concentrations equal or higher than 5 wt% and attributed to the inefficient blending of composites using melt extrusion or solvent casting method [11, 19]. Whereas, the current blending procedure is even effective at 0.25 wt% of MFC/NFC to act as nucleating agents.

From the second heating cycle (Figure 3b and 3d), almost similar melting temperatures were observed for neat PHB, P-PHB and all PHB-NFC/MFC masterbatches, indicating no PHB degradation during the processing. Interestingly, no cold crystallization peak (T_{cc}) was observed for PHB-NFC masterbatches indicating the complete crystallization of PHB during the previous cooling cycle. In contrast, an under-developed cold crystallization peak was observed for PHB-MFC masterbatches indicating partial crystallization of PHB, in response to the coarser and heterogeneous MFC morphology that hindered the PHB crystallization due to restriction in PHB polymeric chain movement. In addition, no clear T_g was observed for PHB-NFC/MFC masterbatches that might also be attributed to the nucleating ability of fibers. The effect of fiber concentrations were also correlated with the overall crystallinity X_c of the nanocomposite materials (Table 2), where an increase in the fiber content first increases the crystallinity X_c and later decreases due to the disturbance in the regularity of PHB chains resulting in hindrance of crystallization with the fiber overloading. In contrast, a continuous reduction in crystallinity was reported for composites of PHB-MCC (5 to 20 wt%) or PCL-CNC/MFC (9 wt%) as the starting weight fraction of fibers already exceeded the threshold concentration and hence overloaded the polymer matrix [11, 30]. As such, PHB-NFC was observed with the highest crystallinity of 37.68% at 0.50 wt% of NFC comparing PHB-MFC with a maximum crystallinity of 35.29% at 2 wt% of MFC. Therefore, the fiber concentration corresponding with a maximum crystallinity was considered as the threshold limit of fibers to be added into the PHB matrix i.e. 0.50 wt% for NFC and 2 wt% for MFC. This observation is attributed to the smaller fiber diameters and relatively more fibrillated morphology of NFC (higher surface area) than MFC [22] that provided more nuclei for better PHB crystallization. Similarly, higher crystallinities were reported for PCL-CNC due to higher surface area of CNC than PCL-MFC at the same fiber loading [30].

3.3. Isothermal crystallization of PHB-NFC/MFC masterbatches using the Avrami kinetics

The isothermal crystallization kinetics of neat PHB and PHB-NFC/MFC masterbatches were investigated to give detailed information on the effects of fibers on the crystallization kinetics of PHB.

The evolution of exothermic heat flow as a function of time and at fixed crystallization temperature of 80 °C is depicted in Figure 4a and 4c for neat PHB, P-PHB and PHB-NFC/MFC masterbatches. It is known that a low isothermal crystallization temperature of 80 °C results in a smooth shape of the crystallization exotherm, whereas, temperature ≥90 °C leads to the rather irregular shape of the DSC curve that would interfere in the thermal analysis [41]. Clearly, the exotherm for P-PHB occurred sooner than the neat PHB and mainly attributed to the effect of solvents used during the processing of PHB. It was also clearly evidenced that the addition of fibers in the PHB matrix significantly accelerated the crystallization of PHB, as determined by the smaller experimental values of $t_{1/2\ Iso}$ obtained from the exotherms in comparison to the $t_{1/2\ Iso}$ values of PHB or P-PHB (Table 3). Similar to the trend followed by $t_{1/2\ Non\text{-}Iso}$ values (as seen in section 3.2, Table 2), $t_{1/2\ Iso}$ values also first decreased up to a minimum value and then increased upon the NFC/MFC addition in the PHB masterbatches (as described earlier). In order to compare the extent of PHB crystallization in response to the various fiber fractions of NFC and MFC, the relative degree of crystallinity (X_t) as a function of crystallization time (t) was calculated for each composites as shown in Figure 4b and 4d. It is defined as the ratio of the area under the exothermic curve between the onset crystallization time and the crystallization time t to the whole area under the exothermic curve from the onset to the end of crystallization time, as follows from Equation (4) [30]:

$$X_t = \frac{\int_0^t \left(\frac{dH}{dt}\right) dt}{\int_0^\infty \left(\frac{dH}{dt}\right) dt} \quad (4)$$

where dH/dt is the relative heat flow from the exothermic curve at fixed crystallization temperature of 80 °C.

The curves in Figure 4b and 4d exhibit the typical sigmoidal or S-shape reflecting the three different stages of crystallization i.e. (i) the starting nucleation step, where the development of nuclei take place for further crystallization, (ii) the linear primary crystallization zone, where a radial crystal growth is followed over the nuclei, and (iii) the final secondary crystallization phase, where lamellae thickening is followed [42]. From Figure 4b, P-PHB developed the crystallinity faster than the neat PHB and attributed to the effect of further processing. PHB-NFC/MFC masterbatches developed their respective crystallinity much faster than the neat and P-PHB, with MFC 2 wt% being fastest than other composites (see Figure 4b and 4d inset with detail of first 2 min). Here, the relative degree of crystallinity (X_t) should not be confused with degree of crystallinity (X_c) for composites. Although, MFC 2 and MFC 5 achieved their respective crystallinity earlier than NFC nanocomposites, there crystallinities (X_c) were still lower than PHB-NFC composites due to heterogeneous MFC morphology.

In order to understand why MFC 2 wt% and 5 wt% (smaller surface area) achieved faster PHB crystal-

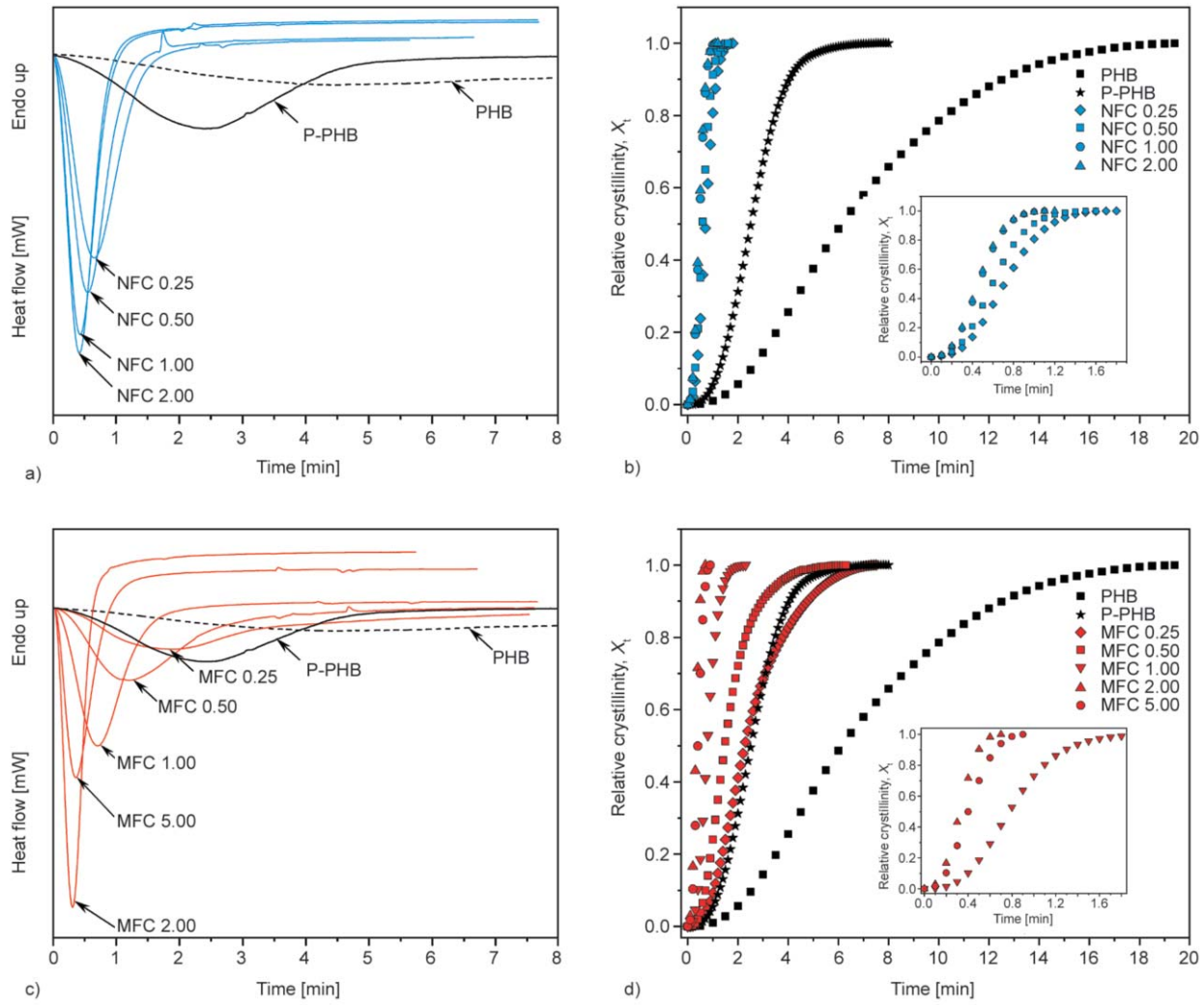

Figure 4. Isothermal DSC curves at a crystallization temperature of 80 °C and evolution of relative crystallinity with crystallization time for neat PHB, P-PHB and PHB-NFC/MFC masterbatches showing (a) crystallization exotherms for PHB-NFC masterbatches, (b) evolution of relative crystallinity for PHB-NFC masterbatches, inset (details of first 2 min) (c) crystallization exotherms for PHB-MFC masterbatches, and (d) evolution of relative crystallinity for PHB-MFC masterbatches, inset (details of first 2 min).

lization than finer NFC 2 wt%, the respective crystallization kinetics were modelled by using the Avrami Equations (5), (6) and (7) [9, 43–45] as follows:

$$1 - X_t = \exp(-kt^n) \tag{5}$$

$$\log\left[-\ln(1 - X_t)\right] = \log k + n \log t \tag{6}$$

$$t_{1/2\ \text{Avrami}} = \left(\frac{\ln 2}{k}\right)^{1/n} \tag{7}$$

where X_t represents the relative crystallinity at time t, k is the Avrami crystallinity rate constant [min^{-n}] and n is the Avrami exponent [46]. When $X_t = 0.50$ in Equation (6) then $t_{1/2\ \text{Avrami}}$ is the half crystallization time i.e. time at which the extent of crystallization is 50% [9].

The Avrami plots of neat PHB, P-PHB, and PHB-NFC/MFC masterbatches are illustrated in Figure 5 for compositions with variable amount of fiber fractions. From the Avrami plots, the values of n and k were calculated from a linear fit of the primary crystallization data points i.e. relative crystallinity in between 3–20%, as it is advisable to neglect the initial data points due to the initial stabilization of the instrument [36]. In addition, the later data points that were attributed to the secondary crystallization were also not taken into consideration due to non-linearity in the plots, as seen from the Figure 5. The calculated Avrami parameters n and k from the linear fit showed a correlation coefficient R^2 in between 0.9994 to 1, and are summarized in Table 3. The Avrami exponent n reflects the shapes of the growing crystals and therefore determine the extent to which crystallization mechanism has altered after blending with additives [47]. As such, for neat PHB, P-PHB, and PHB-NFC masterbatches n varies in between 2.46–2.83, indicating the two-dimensional growth of the crystals with a heterogeneous type of nucleation [48, 49]. The detailed description of various possible values of n is given elsewhere [46]. In addition, a consistent and slightly higher value of n was observed for PHB-NFC masterbatches comparing neat PHB and P-PHB, indicating minor changes in the crystallization mechanism of PHB. However, at a high fiber loading of MFC, i.e. 1 to 5 wt%, the value of n was 3 or higher, indicating the three-dimensional growth of the PHB crystals. This observation can be explained by the broad distribution of MFC diameters that might promote densely packed fiber-networks in PHB matrix and result in a reduction in PHB chain mobility [30]. The broad distribution of MFC diameters may also act as nuclei of different sizes and nucleating abilities that might result in uneven or uncontrolled crystal growth leading to three-dimensional growth of the PHB crystals. Similar observations resulted in a blend of PHB-poly(vinyl acetate), where the value of n varies between 1.8–3.3 depending upon the blend concentration and exhibit two to three-dimensional crystal growth [47]. Therefore, addition of MFC strongly altered the crystallization mechanism of PHB ($n \geq 3$) comparing the NFC in PHB nanocomposites with $n < 3$ and similar to the P-PHB ($n = 2.76$).

From the calculated k values (Table 3) reflecting the crystallization rates, MFC with 2 and 5 wt% fiber fraction in PHB obtained a maximum value of k inferring the fastest crystallization of PHB. This observation was in agreement with the polycaprolactone

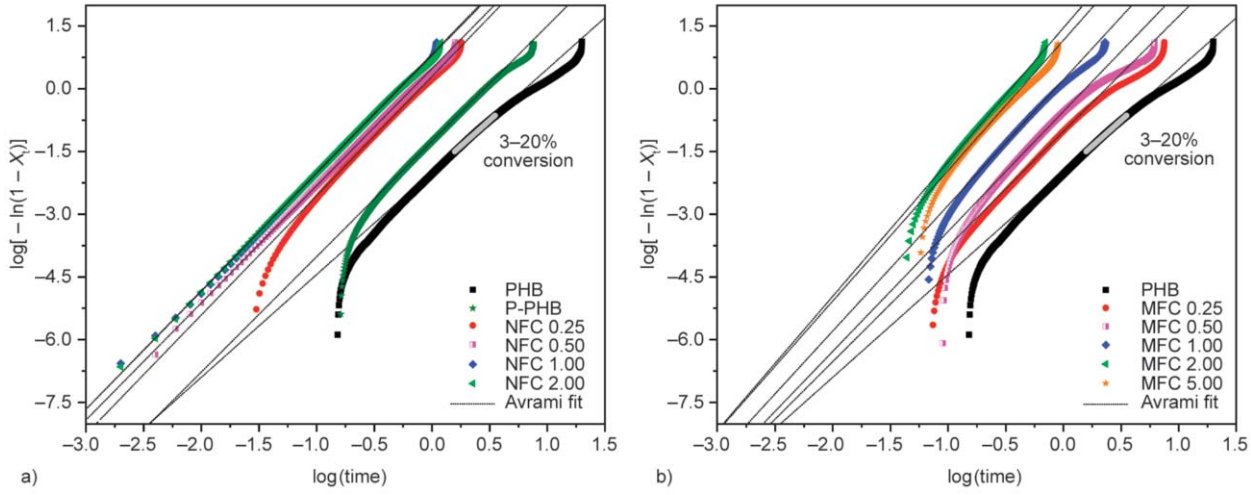

Figure 5. Avrami plots for (a) neat PHB, P-PHB and PHB-NFC masterbatches (b) PHB-MFC masterbatches.

(PCL)-MFC and PCL-cellulose nanowhiskers (CNW) nanocomposites, where, MFC resulted in faster crystallization kinetics than CNW (fine morphology), by requiring lowest bulk activation energy to crystallize PCL [30]. In order to further validate the isothermal crystallization studies of PHB modelled with Avrami's kinetics, half crystallization times ($t_{1/2\ Avrami}$) were calculated from the Avrami parameters (Equation (7)) and compared with the experimental values of $t_{1/2\ Iso}$ obtained from the isothermal tests. From Table 3, the $t_{1/2\ Avrami}$ values are very similar to the experimental $t_{1/2\ Iso}$ values and therefore suggest the suitability of Avrami theory in determining the isothermal crystallization kinetics of PHB-NFC/MFC composites. It would also be interesting to discuss the effect of NFC/MFC on secondary crystallization of PHB that is responsible for the brittle nature of PHB. Clearly, both neat PHB and P-PHB possessed the typical secondary crystallization behaviour as visible from the non-linearity in the plots (see Figure 5a). Similar observations were observed for PHB-MFC composites (see Figure 5b), due to non-homogeneous crystal growths pertaining to heterogeneous MFC morphology. However, blending with the more homogeneous NFC fibers resulted in better linearity of the Avrami plots (above 0.25 wt% of NFC, see Figure 5a) inferring drastic reduction in secondary crystallization of PHB-NFC composites. Therefore, these observations definitely exhibit the suitability of the Avrami theory to determine the crystallization mechanism/kinetics of PHB in presence of various types of nucleating agents with different morphology.

Table 3. Avrami crystallization kinetic parameters (n and k), calculated half crystallization time obtained from Avrami parameters ($t_{1/2\ Avrami}$) and experimental half crystallization time obtained from isothermal tests ($t_{1/2\ Iso}$) for neat PHB, P-PHB and PHB-NFC/MFC nanocomposites with different fiber concentration of 0.25, 0.50, 1, 2 and 5 wt%.

Sample	n±0.01	k±0.003 [min^{-n}]	$t_{1/2\ Avrami}$±0.002 [min]	$t_{1/2\ Iso}$±0.002 [min]
PHB	2.46	0.010	5.601	4.914
P-PHB	2.76	0.055	2.504	2.426
NFC 0.25	2.85	1.966	0.694	0.654
NFC 0.50	2.80	3.016	0.591	0.554
NFC 1.00	2.82	6.242	0.459	0.434
NFC 2.00	2.83	6.733	0.448	0.426
MFC 0.25	2.75	0.096	2.052	1.892
MFC 0.50	2.87	0.286	1.361	1.204
MFC 1.00	3.00	1.635	0.751	0.722
MFC 2.00	3.21	28.517	0.314	0.308
MFC 5.00	3.12	14.401	0.378	0.368

3.4. Morphological analysis of the PHB-NFC/MFC nanocomposite films

The neat PHB, P-PHB and PHB-NFC/MFC nanocomposite films were characterized by the polarized optical microscopy (POM) in order to determine the influences of NFC and MFC addition on the microstructure of PHB crystals, as presented in Figure 6 at two different magnifications. In order to visualize the clear microstructural boundary of single spherulite, PHB films with low NFC/MFC concentration of 0.25 wt% were selected. However, no significant differences in spherulite sizes were observed in the polarized micrographs of PHB films containing higher NFC/MFC fiber fractions, which confirm a good homogeneous mixing at given fiber content. Spherulites with distinct maltese patterns and well-defined boundaries were observed for both neat and P-PHB films due to the highly regular arrangement of pristine PHB polymer chains [50] (Figure 6a–6d). Large individual spherulites with banded terraces around the centre were also observed and attributed to the low nucleation density of PHB [51, 52]. These large spherulites are responsible for the brittle nature of PHB [53]. Qualitatively, no significant differences were observed in the spherulite structure/shape for neat PHB (Figure 6a, 6b) and P-PHB (Figure 6c, 6d) indicating the unaltered PHB crystallization mechanism after the processing (as seen previously from Avrami kinetics i.e. $n < 3$ accounting for the two-dimensional growth of crystals). Similarly, with the addition of NFC in the PHB matrix the spherulite structure remained almost similar to the PHB or P-PHB, due to the comparable crystallization mechanism ($n < 3$). However, addition of NFC in the PHB matrix (0.25 wt%) drastically reduced the spherulite size along with increment in spherulites number (see Figure 6e and 6f). This effect is attributed to the presence of NFC as a heterogeneous nucleating agent (even at low concentrations) which resulted in spherulites of uniform and smaller sizes (see Figure 6e). Due to the high nucleation density in presence of NFC, the radial growth of PHB spherulites ceased early as they contacted each other and retarded the initiation for the growth of secondary spherulites (also confirmed from Figure 5a), responsible for the brittle nature of PHB. Addition of MFC also resulted in the reduction of spherulite size and

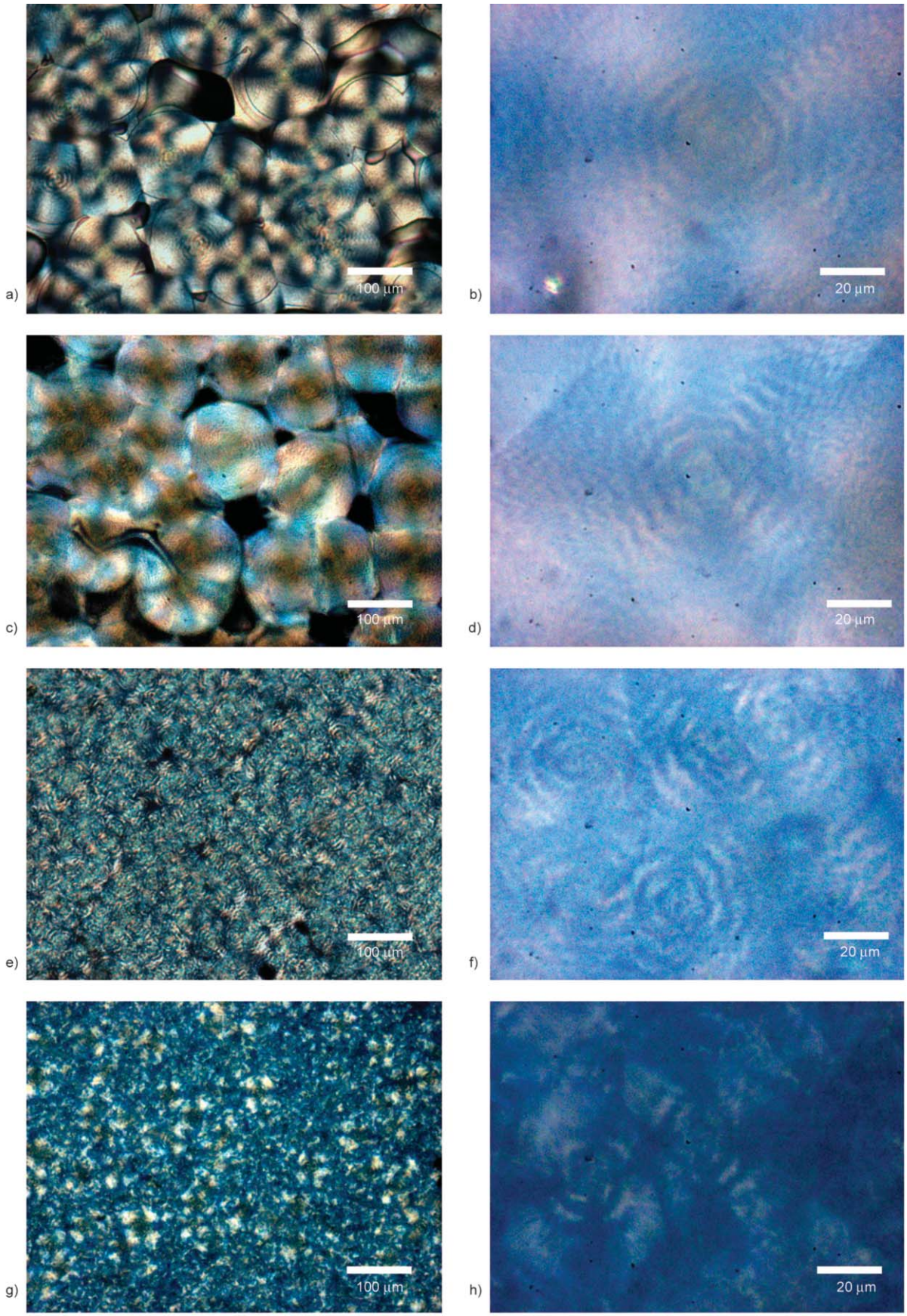

Figure 6. Polarized optical micrographs of (a) neat PHB film at 10×, (b) neat PHB film at 50×, (c) P-PHB film at 10×, (d) P-PHB film at 50×, (e) NFC 0.25 film at 10×, (f) NFC 0.25 film at 50×, (g) MFC 0.25 film at 10×, and (h) MFC 0.25 film at 50×.

increment of spherulite numbers (as seen from Figure 6g and 6h) that also confirmed the nucleating ability of MFC when blended in PHB matrix. However, the bigger MFC size in comparison to NFC hindered the mobility of PHB chains and resulted in a distorted spherulite shape due to typical twisting of the crystal lamellae (see Figure 6h) (in agreement with the previous observations, $n \geq 3$ i.e. crystallization mechanism of PHB altered strongly). The driving force of this distortion in spherulites is mainly explained by the anisotropic and unbalanced surface stresses in the polymer [54], which in present case originated from the broad distribution of MFC acting as nuclei with different nucleating abilities and resulted in spherulites of non-homogeneous sizes (see Figure 6g).

The fracture morphology of PHB-NFC/MFC films as observed by SEM studies is shown in Figure 7. For P-PHB films, a clean, a smooth and compact surface was observed. With the addition of NFC, the PHB films containing low (0.25 wt%) and high NFC fractions (2.00 wt%) became little bulkier and appeared with uniform fractured surface along with some textures due to the fiber distribution (Figure 7b,

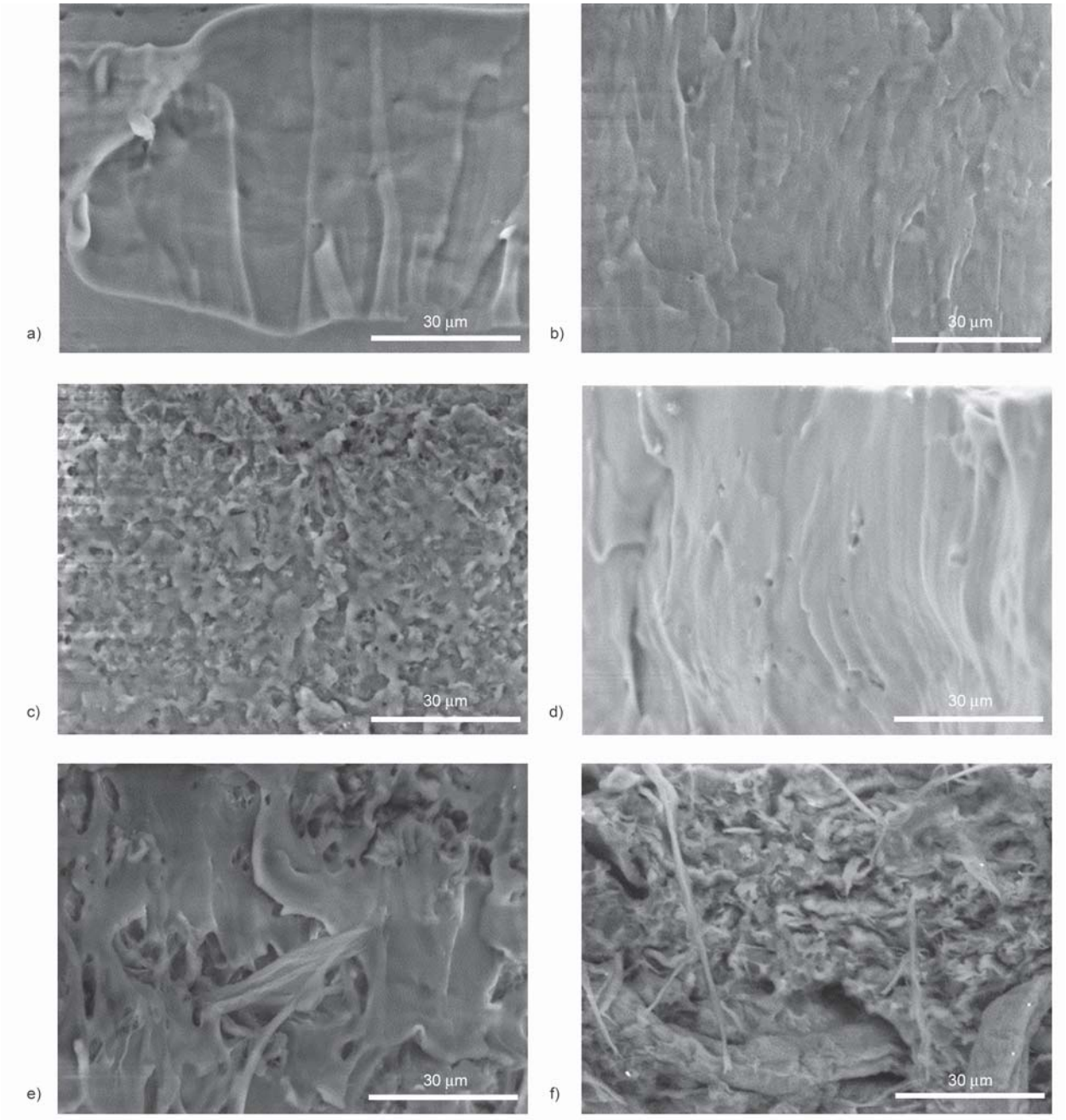

Figure 7. SEM of fractured PHB films showing (a) P-PHB, (b) NFC 0.25, (c) NFC 2.00, (d) MFC 0.25, (e) MFC 2.00, (f) MFC 5.00.

7c). As such, the role of single NFC fiber network was clearly visible in the PHB-NFC films and attributed to the uniform blending procedure and dense fiber network (Figure 7c). Notably, because of good dispersion of NFC in PHB matrix over a broad concentration range, NFC was acting as an efficient nucleating agent even at lower concentrations of 0.25 or 0.50 wt%, up to 2 wt%. In case of PHB-MFC films, the fractured surface at high fiber fraction (2 and 5 wt%) (Figure 7e, 7f) clearly showed numerous fiber pull-outs resulting from the poor MFC-PHB interfacial adhesion. Interestingly, blending with only 5 wt% MFC was observed as overloading in PHB matrix (Figure 6f) that certainly exhibited the unique ability of the developed processing procedure in uniformly mixing a hydrophilic filler with a hydrophobic matrix at this low fiber concentrations.

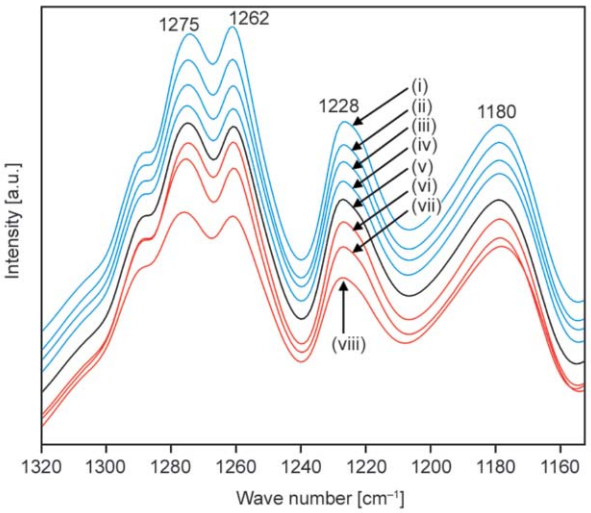

Figure 8. FTIR spectra showing detailed spectra in wave number range 1400-1100 cm^{-1} for (i) NFC 0.50, (ii) NFC 0.25, (iii) NFC 1.00, (iv) NFC 2.00, (v) P-PHB, (vi) MFC 2.00, (vii) MFC 0.25 and (viii) MFC 5.00 wt%.

3.5. Chemical analysis of PHB-NFC/MFC composite films

The PHB-NFC/MFC composite films were characterized by Fourier-transform infrared (FTIR) spectroscopy to evaluate the influences of fibers and their concentrations on the crystalline and amorphous bands of PHB. The major characteristics absorption bands for PHB are as follows: 1721 cm^{-1} (C=O asymmetrical stretching), 1687 cm^{-1} (C=O symmetrical stretching), 1453 cm^{-1} (CH_3 asymmetric stretching), 1380 cm^{-1} (CH_3 symmetric stretching), 1275 cm^{-1} (CH_2 wagging), 1262 cm^{-1} (C–O–C stretching with C–H deformation), 1228 cm^{-1} (C–CH_3 stretching), and1180 cm^{-1} (C-O-C asymmetric stretching) [55–57]. All spectra were baseline corrected and normalized on the 1453 cm^{-1} band, which is considered insensitive for changes in crystallinity [56].

From Figure 8, the wavenumber region 1100–1400 cm^{-1} is detailed for a qualitative analysis of crystallinity for PHB-NFC/MFC composite films. The absorption intensity of bands at 1275 and 1228 cm^{-1} (crystalline bands) and 1180 cm^{-1} (amorphous band) is sensitive to the degree of crystallinity [56]. In present case of semi-crystalline PHB, all three bands are present, while in fully-crystalline PHB, only the 1228 cm^{-1} band is present and assigned to the conformation of the PHB helical chains [56]. Considerable differences were observed in the intensity ratio I_{1228}/I_{1453} (crystalline index): the crystallinity index equals 4.75 (PHB), 4.76 (P-PHB), 5.00 (NFC 0.25), 5.13 (NFC 0.50), 4.88 (NFC 1.00), 4.74 (NFC 2.00), 4.51 (MFC 0.25), 4.77 (MFC 2.00) and 3.86 (MFC 5.00). Clearly, the crystallinity of all PHB-NFC films are higher than PHB-MFC films, where, NFC 0.50 wt% obtained the highest value and MFC 5.00 wt% obtained the lowest value of crystallinity. This trend is in agreement with the previous values for the degree of crystallinity (X_c) calculated from non-isothermal DSC analysis of PHB-NFC/MFC masterbatches.

3.6. Mechanical properties of PHB-NFC/MFC films

The PHB-NFC/MFC films were examined for the effect of NFC/MFC and their concentrations on the mechanical properties of nanocomposite films. Figure 9a shows the stress-strain curve for PHB-NFC films. Mechanical performance in terms of tensile strength, Young's modulus and elongation at break for neat PHB, P-PHB, and PHB-NFC/MFC films is shown in Figure 9b–9d.

The P-PHB presented slightly superior mechanical properties compared to the neat PHB despite of having similar values for crystallinity (Table 2). This might be attributed to an increase in the final crystallinity of P-PHB film when stored for 7 days prior to mechanical testing, as P-PHB crystallizes faster than the PHB due to solvent processing (as seen from half crystallization times, Table 3). The tensile strength of both PHB and P-PHB film is inferior to the PHB-NFC/MFC films and is attributed to the formation of large spherulites (Figure 6) with cracks

and splitting, which depend on lower nucleation density [2, 53]. However, after adding NFC/MFC in PHB matrix, tensile strength of composites is improved relatively to PHB or P-PHB, due to the reinforcing and nucleating effect of fibers. With the increasing NFC concentrations (0.25–2 wt%), tensile strength of films continuously increased. In contrast, at higher MFC fraction in film (1 to 5 wt%), tensile strength decreased which may attributed to the increased non-homogeneity in spherulites sizes upon fiber loading in the matrix.

Several publications reported that the Young's modulus (measure of stiffness) of composites increases and the corresponding elongation at break decreases with the addition of micro/nano-scale reinforcements in polymer matrix [32, 33]. In contrast, the present PHB-NFC films clearly show the highest elongation at break (or reduction in brittleness) compared to the neat PHB, P-PHB or PHB-MFC films and hence provide lower Young modulus values. Whereas, PHB-MFC films show either equal or slightly larger values of Young modulus than P-PHB or PHB-NFC films and therefore do not improve flexibility or elongation at break of films. These observations directly correlate with the ability of NFC or MFC to hinder secondary crystallization in PHB polymer: during secondary crystallization, new, thin spherulites are formed from the amorphous regions that lead to increase in crystallinity, stress and Young modulus and decrease in elongation at break, resulting the material to be hard and brittle [2, 53]. This observation is in line with the previous characterization where NFC occurred as a better nucleating agent for PHB, resulting in smaller and incremented number of spherulites that hindered the formation of secondary spherulites (confirmed by Figure 5a). Consequently,

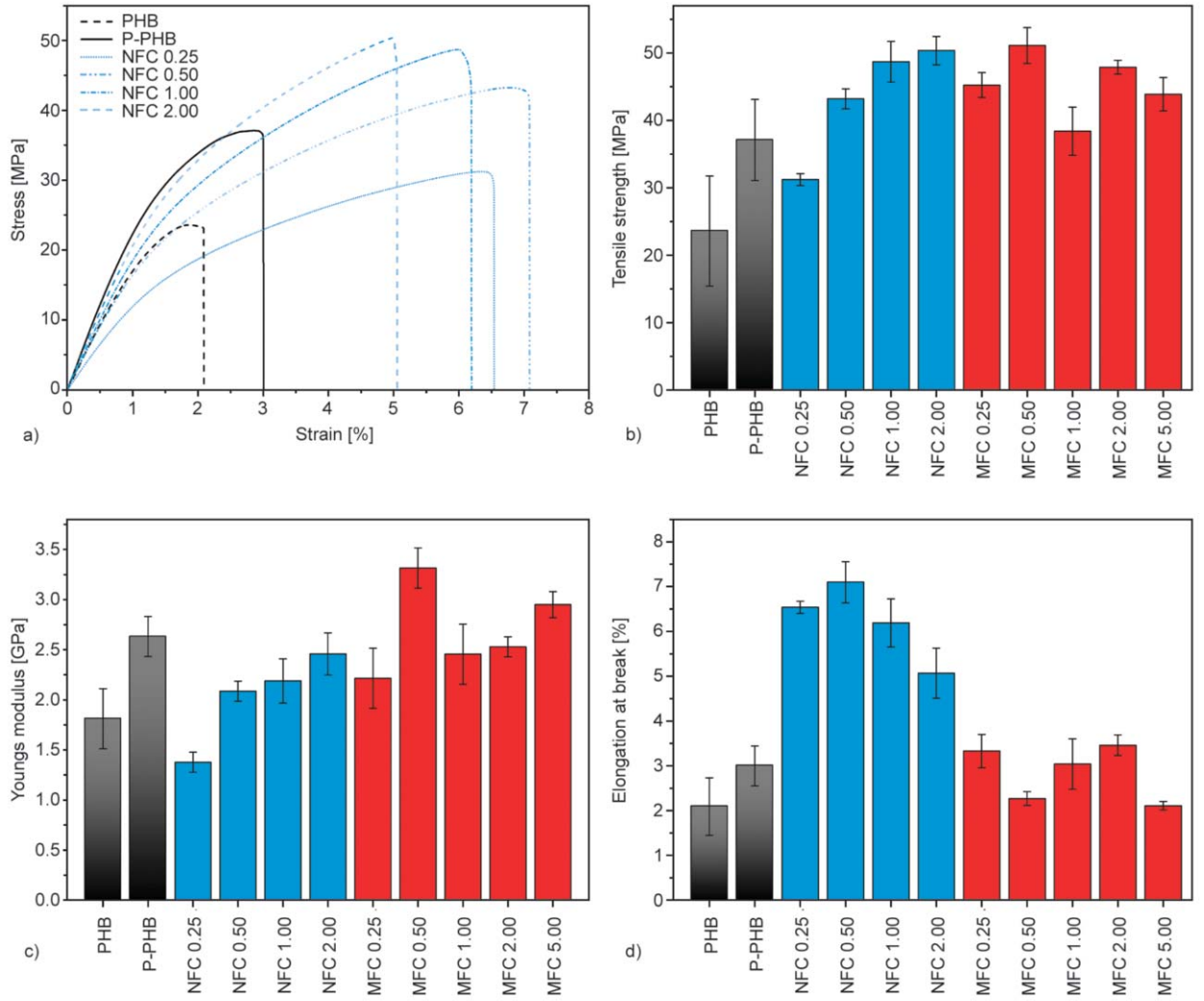

Figure 9. Mechanical properties of neat PHB, P-PHB and PHB-NFC/MFC films based on micro-tensile test (a) stress-strain curve for PHB-NFC films, (b) tensile strength, (c) Young's modulus, and (d) elongation at break.

PHB-NFC films remain flexible due to the presence of more amorphous regions that are responsible for providing ductility to the polymers [58]. Whereas, addition of MFC in PHB matrix resulted in a distorted PHB crystal shape, non-homogeneous spherulites (as seen from POM images, Figure 6g, 6h) and consequently exhibited secondary crystallization behaviour (Figure 5b), resulting in brittle PHB-MFC films. In order words, it is also possible that during storage of films for 7 days the crystallinity of all films increases by secondary crystallization except for PHB-NFC films, therefore providing relatively more flexible films than others [37].

4. Conclusions

A chlorinated-solvent-free based approach was developed to achieve homogenous dispersion of polar NFC/MFC in non-polar PHB matrix that resulted in fully bio-based nanocomposite materials (masterbatches). Through compression moulding, the prepared masterbatches were transformed into free-standing films. The effects of NFC and MFC fibers on the crystallization behaviour of PHB films was studied using DSC and POM. In presence of NFC and to a lesser extent MFC, crystallinity index of the matrix increases, suggesting a nucleating effect of the cellulose fillers in relation to surface area (NFC > MFC). However, after reaching their respective maximum crystallinities at the threshold concentration i.e. 0.5 wt% for NFC and 2 wt% for MFC, the crystallinities dropped with the further addition of fiber to PHB matrix, accounting for the restriction in the mobility of PHB chains due to fiber over loading. At a fixed crystallization temperature of 80 °C, the crystallization kinetics was largely accelerated with both NFC and MFC, this effect being slightly more marked with MFC due to the broad distribution of MFC diameters promoting uneven or uncontrolled crystal growth in three-dimensions ($n > 3$). Therefore, PHB-MFC nanocomposites unveils the maximum changes in the crystallization mechanism of PHB comparing PHB-NFC composites with $n < 3$. Due to the fine morphology of NFC and narrow diameters distribution, large number of well dispersed spherulites were observed from POM images. In addition to, MFC resulted distorted spherulite shape due to larger fiber morphology and affected the crystallization kinetics most. Through mechanical testing of films, NFC was considered as a suitable bio-based nano-filler choice for reducing the brittleness of the PHB film, as seen by highest elongation at break comparing the neat PHB and PHB-MFC films. Consistent with this result, no growth of secondary crystals was visible after addition of NFC in PHB matrix (Avrami plots), whereas, MFC promoted secondary crystallization in PHB matrix and hence remained more brittle than PHB-NFC films. The variations in the crystallinities of PHB-NFC/MFC films were also confirmed by FTIR analysis and correlated well with the crystallinities obtained by DSC measurements.

Acknowledgements

This work was financially sponsored by the Junioprofessorenprogram Baden-Württemberg ‘Functional Bio-based Nano-Coating for Paper Applications”‘ (‘NaCoPa’-project 2012–2015) and the Robert Bosch Foundation in the framework of the Juniorprofessorenprogram ‘Sustainable use of Natural Materials’ (‘Foresnab’-project 2011–2016).

References

[1] Reddy C. S. K., Ghai R., Rashmi, Kalia V. C.: Polyhydroxyalkanoates: An overview. Bioresource Technology, **87**, 137–146 (2003). https://doi.org/10.1016/S0960-8524(02)00212-2

[2] Hobbs J. K., McMaster T. J., Miles M. J., Barham P. J.: Cracking in spherulites of poly(hydroxybutyrate). Polymer, **37**, 3241–3246 (1996). https://doi.org/10.1016/0032-3861(96)88468-0

[3] El-Hadi A., Schnabel R., Straube E., Müller G., Riemschneider M.: Effect of melt processing on crystallization behavior and rheology of poly(3-hydroxybutyrate) (PHB) and its blends. Macromolecular Materials and Engineering, **287**, 363–372 (2002). https://doi.org/10.1002/1439-2054(20020501)287:5<363::AID-MAME363>3.0.CO;2-D

[4] Kulkarni S. O., Kanekar P. P., Jog J. P., Patil P. A., Nilegaonkar S. S., Sarnaik S. S., Kshirsagar P. R.: Characterisation of copolymer, poly (hydroxybutyrate-*co*-hydroxyvalerate) (PHB-*co*-PHV) produced by halomonas campisalis (MCM B-1027), its biodegradability and potential application. Bioresource Technology, **102**, 6625–6628 (2011). https://doi.org/10.1016/j.biortech.2011.03.054

[5] Žagar E., Kržan A., Adamus G., Kowalczuk M.: Sequence distribution in microbial poly(3-hydroxybutyrate-*co*-3-hydroxyvalerate) *co*-polyesters determined by NMR and MS. Biomacromolecules, **7**, 2210–2216 (2006). https://doi.org/10.1021/bm060201g

[6] Choi J. S., Park W. H.: Effect of biodegradable plasticizers on thermal and mechanical properties of poly(3-hydroxybutyrate). Polymer Testing, **23**, 455–460 (2004). https://doi.org/10.1016/J.polymertesting.2003.09.005

[7] Baltieri R. C., Innocentini Mei L. H., Bartoli J.: Study of the influence of plasticizers on the thermal and mechanical properties of poly(3-hydroxybutyrate) compounds. Macromolecular Symposia, **197**, 33–44 (2003). https://doi.org/10.1002/masy.200350704

[8] Jacquel N., Tajima K., Nakamura N., Kawachi H., Pan P., Inoue Y.: Nucleation mechanism of polyhydroxybutyrate and poly(hydroxybutyrate-*co*-hydroxyhexanoate) crystallized by orotic acid as a nucleating agent. Journal of Applied Polymer Science, **115**, 709–715 (2009). https://doi.org/10.1002/app.30873

[9] Kai W., He Y., Inoue Y.: Fast crystallization of poly(3-hydroxybutyrate) and poly(3-hydroxybutyrate-*co*-3-hydroxyvalerate) with talc and boron nitride as nucleating agents. Polymer International, **54**, 780–789 (2005). https://doi.org/10.1002/pi.1758

[10] Ma P., Deshmukh Y. S., Wilsens C. H. R. M., Ryan Hansen M., Graf R., Rastogi S.: Self-assembling process of oxalamide compounds and their nucleation efficiency in bio-degradable poly(hydroxyalkanoate)s. Scientific Reports, **5**, 13280/1–13280/9 (2015). https://doi.org/10.1038/srep13280

[11] El-Hadi A. M.: Influence of microcrystalline cellulose fiber (MCCF) on the morphology of poly(3-hydroxybutyrate) (PHB). Colloid and Polymer Science, **291**, 743–756 (2013). https://doi.org/10.1007/s00396-012-2784-x

[12] Rajan R., Sreekumar P. A., Joseph K., Skrifvars M.: Thermal and mechanical properties of chitosan reinforced polyhydroxybutyrate composites. Journal of Applied Polymer Science, **124**, 3357–3362 (2012). https://doi.org/10.1002/app.35341

[13] El-Hadi M. A.: Investigation of the effect of nano-clay type on the non-isothermal crystallization kinetics and morphology of poly(3(R)-hydroxybutyrate) PHB/clay nanocomposites. Polymer Bulletin, **71**, 1449–1470 (2014). https://doi.org/10.1007/s00289-014-1135-0

[14] Botana A., Mollo M., Eisenberg P., Torres Sanchez R. M.: Effect of modified montmorillonite on biodegradable PHB nanocomposites. Applied Clay Science, **47**, 263–270 (2010). https://doi.org/10.1016/j.clay.2009.11.001

[15] Shan G-F., Gong X., Chen W-P., Chen L., Zhu M-F.: Effect of multi-walled carbon nanotubes on crystallization behavior of poly(3-hydroxybutyrate-*co*-3-hydroxyvalerate). Colloid and Polymer Science, **289**, 1005–1014 (2011). https://doi.org/10.1007/s00396-011-2412-1

[16] Bhardwaj R., Mohanty A. K., Drzal L. T., Pourboghrat F., Misra M.: Renewable resource-based green composites from recycled cellulose fiber and poly(3-hydroxybutyrate-*co*-3-hydroxyvalerate) bioplastic. Biomacromolecules, **7**, 2044–2051 (2006). https://doi.org/10.1021/bm050897y

[17] Barkoula N. M., Garkhail S. K., Peijs T.: Biodegradable composites based on flax/polyhydroxybutyrate and its copolymer with hydroxyvalerate. Industrial Crops and Products, **31**, 34–42 (2010). https://doi.org/10.1016/j.indcrop.2009.08.005

[18] Alemdar A., Sain M.: Biocomposites from wheat straw nanofibers: Morphology, thermal and mechanical properties. Composites Science and Technology, **68**, 557–565 (2008). https://doi.org/10.1016/j.compscitech.2007.05.044

[19] Yu H-Y., Qin Z-Y., Zhou Z.: Cellulose nanocrystals as green fillers to improve crystallization and hydrophilic property of poly(3-hydroxybutyrate-*co*-3-hydroxyvalerate). Progress in Natural Science: Materials International, **21**, 478–484 (2011). https://doi.org/10.1016/S1002-0071(12)60086-0

[20] Yu H., Yan C., Yao J.: Fully biodegradable food packaging materials based on functionalized cellulose nanocrystals/poly(3-hydroxybutyrate-*co*-3-hydroxyvalerate) nanocomposites. RSC Advances, **4**, 59792–59802 (2014). https://doi.org/10.1039/c4ra12691b

[21] Syverud K., Stenius P.: Strength and barrier properties of MFC films. Cellulose, **16**, 75–85 (2009). https://doi.org/10.1007/s10570-008-9244-2

[22] Kumar V., Bollström R., Yang A., Chen Q., Chen G., Salminen P., Bousfield D., Toivakka M.: Comparison of nano- and microfibrillated cellulose films. Cellulose, **21**, 3443–3456 (2014). https://doi.org/10.1007/s10570-014-0357-5

[23] Missoum K., Belgacem M. N., Bras J.: Nanofibrillated cellulose surface modification: A review. Materials, **6**, 1745–1766 (2013). https://doi.org/10.3390/ma6051745

[24] Abdul Khalil H. P. S., Davoudpour Y., Islam M. N., Mustapha A., Sudesh K., Dungani R., Jawaid M.: Production and modification of nanofibrillated cellulose using various mechanical processes: A review. Carbohydrate Polymers, **99**, 649–665 (2014). https://doi.org/10.1016/j.carbpol.2013.08.069

[25] Rastogi V. K., Samyn P.: Novel production method for *in-situ* hydrophobization of a microfibrillated cellulose network. Materials Letters, **120**, 196–199 (2014). https://doi.org/10.1016/j.matlet.2014.01.060

[26] Bazzo G. C., Caetano D. B., Boch M. L. T., Mosca M., Branco L. C., Zétola M., Pereira E. M., Pezzini B. R.: Enhancement of felodipine dissolution rate through its incorporation into Eudragit® E–PHB polymeric microparticles: *In vitro* characterization and investigation of absorption in rats. Journal of Pharmaceutical Sciences, **101**, 1518–1523 (2012). https://doi.org/10.1002/jps.23044

[27] Fiorese M. L., Freitas F., Pais J., Ramos A. M., de Aragão G. M. F., Reis M. A. M.: Recovery of polyhydroxybutyrate (PHB) from *Cupriavidus necator* biomass by solvent extraction with 1,2-propylene carbonate. Engineering in Life Sciences, **9**, 454–461 (2009). https://doi.org/10.1002/elsc.200900034

[28] Bayardon J., Holz J., Schäffner B., Andrushko V., Verevkin S., Preetz A., Börner A.: Propylene carbonate as a solvent for asymmetric hydrogenations. Angewandte Chemie International Edition, **46**, 5971–5974 (2007). https://doi.org/10.1002/anie.200700990

[29] Smith B., Morely J., Sathish A., Rahman A., Sims R. C., Miller C. D.: Propylene carbonate extraction for recovery of poly-3-hydroxybutryate. in 'SBI Science and Technology Review, Logan, Utah, United States of America' p1 (2013).

[30] Siqueira G., Fraschini C., Bras J., Dufresne A., Prud'homme R., Laborie M-P.: Impact of the nature and shape of cellulosic nanoparticles on the isothermal crystallization kinetics of poly(ε-caprolactone). European Polymer Journal, **47**, 2216–2227 (2011). https://doi.org/10.1016/j.eurpolymj.2011.09.014

[31] Azizi Samir M. A. S., Alloin F., Sanchez J-Y., Dufresne A.: Cellulose nanocrystals reinforced poly(oxyethylene). Polymer, **45**, 4149–4157 (2004). https://doi.org/10.1016/j.polymer.2004.03.094

[32] Pandey J. K., Lee C. S., Ahn S-H.: Preparation and properties of bio-nanoreinforced composites from biodegradable polymer matrix and cellulose whiskers. Journal of Applied Polymer Science, **115**, 2493–2501 (2010). https://doi.org/10.1002/app.31205

[33] Lu J., Wang T., Drzal L. T.: Preparation and properties of microfibrillated cellulose polyvinyl alcohol composite materials. Composites Part A: Applied Science and Manufacturing, **39**, 738–746 (2008). https://doi.org/10.1016/j.compositesa.2008.02.003

[34] S. de O. Patrício P., Pereira F. V., dos Santos M. C., de Souza P. P., Roa J. P. B., Orefice R. L.: Increasing the elongation at break of polyhydroxybutyrate biopolymer: Effect of cellulose nanowhiskers on mechanical and thermal properties. Journal of Applied Polymer Science, **127**, 3613–3621 (2013). https://doi.org/10.1002/app.37811

[35] Chen Y., Park Y., Noda I., Jung Y. M.: Influence of polyethylene glycol (PEG) chain length on the thermal behavior of spin-coated thin films of biodegradable poly(3-hydroxybutyrate-*co*-3-hydroxyhexanoate)/PEG blends. Journal of Molecular Structure, **1124**, 159–163 (2016). https://doi.org/10.1016/J.molstruc.2016.02.059

[36] Lorenzo A. T., Arnal M. L., Albuerne J., Müller A. J.: DSC isothermal polymer crystallization kinetics measurements and the use of the avrami equation to fit the data: Guidelines to avoid common problems. Polymer Testing, **26**, 222–231 (2007). https://doi.org/10.1016/j.polymertesting.2006.10.005

[37] Lopera-Valle A., Caputo J. V., Leão R., Sauvageau D., Luz S. M., Elias A.: Influence of epoxidized canola oil (eCO) and cellulose nanocrystals (CNCs) on the mechanical and thermal properties of polyhydroxybutyrate (PHB)–poly(lactic acid) (PLA) blends. Polymers, **11**, 933/1–933/18 (2019). https://doi.org/10.3390/polym11060933

[38] Rastogi V. K., Samyn P.: Bio-based coatings for paper applications. Coatings, **5**, 887–930 (2015). https://doi.org/10.3390/coatings5040887

[39] Rastogi V. K., Samyn P.: Synthesis of polyhydroxybutyrate particles with micro-to-nanosized structures and application as protective coating for packaging papers. Nanomaterials, **7**, 5/1–5/18 (2017). https://doi.org/10.3390/nano7010005

[40] Chen Y., Noda I., Jung Y. M.: Revealing thermal behavior of poly(3-hydroxybutyrate-*co*-3-hydroxyhexanoate) and its polyethylene glycol blends thin films: Effect of 3-hydroxyhexanoate comonomer content. Journal of Molecular Structure, **1162**, 140–144 (2018). https://doi.org/10.1016/j.molstruc.2018.02.053

[41] Di Lorenzo M. L., Sajkiewicz P., La Pietra P., Gradys A.: Irregularly shaped DSC exotherms in the analysis of polymer crystallization. Polymer Bulletin, **57**, 713–721 (2006). https://doi.org/10.1007/s00289-006-0621-4

[42] Rybnikář F.: Mechanism of secondary crystallization in polymers. Journal of Polymer Science Part A: General Papers, **1**, 2031–2038 (1963). https://doi.org/10.1002/pol.1963.100010620

[43] Avrami M.: Kinetics of phase change. I General theory. The Journal of Chemical Physics, **7**, 1103–1112 (1939). https://doi.org/10.1063/1.1750380

[44] Avrami M.: Kinetics of phase change. II Transformation-time relations for random distribution of nuclei. The Journal of Chemical Physics, **8**, 212–224 (1940). https://doi.org/10.1063/1.1750631

[45] Avrami M.: Granulation, phase change, and microstructure kinetics of phase change. III. The Journal of Chemical Physics, **9**, 177–184 (1941). https://doi.org/10.1063/1.1750872

[46] Liu J., Qiu Z., Jungnickel B-J.: Crystallization and morphology of poly(vinylidene fluoride)/poly(3-hydroxybutyrate) blends. III. Crystallization and phase diagram by differential scanning calorimetry. Journal of Polymer Science Part B: Polymer Physics, **43**, 287–295 (2005). https://doi.org/10.1002/polb.20274

[47] Madbouly S. A., Mansour A. A., Abdou N. Y.: Crystallization kinetics of PHB/PVAc blends using time resolved dielectric spectroscopy. European Polymer Journal, **43**, 3933–3942 (2007). https://doi.org/10.1016/j.eurpolymj.2007.06.020

[48] Owen A. J., Heinzel J., Škrbić Ž., Divjaković V.: Crystallization and melting behaviour of PHB and PHB/HV copolymer. Polymer, **33**, 1563–1567 (1992). https://doi.org/10.1016/0032-3861(92)90139-N

[49] Canetti M., Urso M., Sadocco P.: Influence of the morphology and of the supermolecular structure on the enzymatic degradation of bacterial poly(3-hydroxybutyrate). Polymer, **40**, 2587–2594 (1999). https://doi.org/10.1016/S0032-3861(98)00503-5

[50] Drzal L., Misra M., Mohanty A.: Sustainable biodegradable green nanocomposites from bacterial bioplastic for automotive applications. in 'Proceedings of the US EPA 2004 STAR progress review workshop – nanotechnology and the environment II. Philadelphia USA' R830904 (2004).

[51] Xu J., Guo B-H., Chen G-Q., Zhang Z-M.: Terraces on banded spherulites of polyhydroxyalkanoates. Journal of Polymer Science Part B: Polymer Physics, **41**, 2128–2134 (2003). https://doi.org/10.1002/polb.10556

[52] Barham P. J., Keller A.: The relationship between microstructure and mode of fracture in polyhydroxybutyrate. Journal of Polymer Science Part B: Polymer Physics, **24**, 69–77 (1986). https://doi.org/10.1002/polb.1986.180240108

[53] El-Hadi A., Schnabel R., Straube E., Müller G., Henning S.: Correlation between degree of crystallinity, morphology, glass temperature, mechanical properties and biodegradation of poly (3-hydroxyalkanoate) PHAs and their blends. Polymer Testing, **21**, 665–674 (2002). https://doi.org/10.1016/S0142-9418(01)00142-8

[54] Xu J., Ye H., Zhang S., Guo B., Xu J., Ye H., Zhang S., Guo B.: Organization of twisting lamellar crystals in birefringent banded polymer spherulites: A mini-review. Crystals, **7**, 241/1–241/19 (2017). https://doi.org/10.3390/cryst7080241

[55] Wróbel-Kwiatkowska M., Żuk M., Szopa J., Dymińska L., Mączka M., Hanuza J.: Poly-3-hydroxy butyric acid interaction with the transgenic flax fibers: FT-IR and raman spectra of the composite extracted from a GM flax. Spectrochimica Acta Part A: Molecular and Biomolecular Spectroscopy, **73**, 286–294 (2009). https://doi.org/10.1016/j.saa.2009.02.034

[56] Xu J., Guo B-H., Yang R., Wu Q., Chen G-Q., Zhang Z-M.: *In situ* FTIR study on melting and crystallization of polyhydroxyalkanoates. Polymer, **43**, 6893–6899 (2002). https://doi.org/10.1016/S0032-3861(02)00615-8

[57] Chan R. T. H., Garvey C. J., Marçal H., Russell R. A., Holden P. J., Foster L. J. R.: Manipulation of polyhydroxybutyrate properties through blending with ethylcellulose for a composite biomaterial. International Journal of Polymer Science, **2011**, 1–8 (2011). https://doi.org/10.1155/2011/651549

[58] Anbukarasu P., Sauvageau D., Elias A.: Tuning the properties of polyhydroxybutyrate films using acetic acid *via* solvent casting. Scientific Reports, **5**, 17884/1–17884/14 (2016). https://doi.org/10.1038/srep17884